Journal of Alloys and Compounds 509 (2011) 5280–5284

Contents lists available at ScienceDirect

Journal of Alloys and Compounds

journal homepage: www.elsevier.com/locate/jallcom

Electrochemical hydrogen storage properties of non-stoichiometric $La_{0.7}Mg_{0.3-x}Ca_xNi_{2.8}Co_{0.5}$ ($x = 0$–0.10) electrode alloys

Zhenwei Dong[a,b], Yaoming Wu[b], Liqun Ma[a,*], Lidong Wang[b], Xiaodong Shen[a], Limin Wang[b,**]

[a] College of Material Science and Engineering, Nanjing University of Technology, Nanjing 210009, China
[b] State Key Laboratory of Rare Earth Resource Utilization, Changchun Institute of Applied Chemistry, CAS, Changchun 130022, China

ARTICLE INFO

Article history:
Received 3 November 2010
Received in revised form
22 November 2010
Accepted 23 November 2010
Available online 30 November 2010

Keywords:
Alloy electrode
Hydrogen storage
Cycle stability
Electrochemical kinetics

ABSTRACT

The microstructure and electrochemical hydrogen storage characteristics of $La_{0.7}Mg_{0.3-x}Ca_xNi_{2.8}Co_{0.5}$ ($x = 0$, 0.05 and 0.10) alloys prepared by arc-melting and subsequent powder sintering method are investigated. The electrochemical measurement results show that the cycle stability after 100 charge/discharge cycles first increases from 46.4% ($x = 0$) to 54.3% ($x = 0.05$), then decreases to 43.2% ($x = 0.10$), and the high rate dischargeability increases from 64.5% ($x = 0$) to 68.5% ($x = 0.10$) at the discharge current density of 1200 mA/g. The electrochemical impedance spectroscopy analysis indicates that the electrochemical kinetics of the alloy electrodes is improved by increasing Ca. The entire results exhibit that a suitable content of Ca ($x = 0.05$) can improve the overall electrochemical hydrogen storage characteristics of the alloys.

1. Introduction

Energy and environmental protection have become two major themes in today's world, and development for environment friendly energy materials is the prime objective. Hydrogen storage alloys as negative materials of metal hydride–nickel (MH/Ni) secondary batteries are one kind of environment friendly energy storage materials. In recent years, La–Mg–Ni system hydrogen storage alloys have been paid wide attention and considered as one of the novel candidates for negative electrode materials of AB_5-type alloys due to their larger discharge capacities [1–5].

The main problem for La–Mg–Ni system hydrogen storage alloys to be used for industrialization is the poor cycle stability now. Due to Ca and Mg elements belong to the same group (group IIA) in the periodic table and the electro-negativity of Ca is more negative than Mg, it is significant to study the effect of substituting Mg with Ca in the alloys on microstructure and electrochemical characteristics of AB_3-type hydrogen storage alloys.

In this work, we select the $La_{0.7}Mg_{0.3}Ni_{2.8}Co_{0.5}$ alloy as a basic alloy and study the microstructure and electrochemical hydrogen storage characteristics of La–Mg–Ni system $La_{0.7}Mg_{0.3-x}Ca_xNi_{2.8}Co_{0.5}$ ($x = 0$, 0.05 and 0.10) alloys.

2. Experimental

2.1. Alloy preparation and crystallographic characteristics analysis

The La–Ni–Co alloys were prepared by arc-melting under Ar atmosphere, with the constituent metals (La, Ni and Co; >99.9 wt.% purity) on a water-cooled copper hearth. The alloys were turned over and melted three times to make them homogeneous. Then parts of the alloys were crushed and grinded to powder for composites and powder sintering. Before powder sintering, the La–Ni–Co alloys, $CaNi_3$, $MgNi_2$ and Ni powders (200–300 mesh) at a certain molar ratio were pre-mixed using a planetary ball mill QM-1 SP for 10 min under Ar atmosphere. The ball to powder mass ratio was 5:1 and the rotation speed was 200 rpm. After the milling, the mixtures were cold pressed into green compacts under a pressure of 20 MPa. The green compacts were then powder sintered under Ar atmosphere for 12 h at 1273 K.

The $La_{0.7}Mg_{0.3-x}Ca_xNi_{2.8}Co_{0.5}$ ($x = 0$–0.10) hydrogen storage alloys were mechanically crushed into powders of 200–300 mesh in a glove box under a dry Ar atmosphere. XRD measurements were carried out using a Rigaku D/Max-3B diffractometer with CuKα radiation at 40 kV and 30 mA.

2.2. Electrochemical measurements

The testing electrodes were constructed by mixing the composite powders with carbonyl nickel powders at a weight ratio of 1:5. The powder mixtures were pressed into a small pellet under a pressure of 20 MPa. Electrochemical charge/discharge testing was carried out at 298 K by using a DC-5 battery testing system. The electrolyte was 6 M KOH aqueous solution. In each charge/discharge cycle test, the negative electrodes were charged for 7 h at 60 mA/g and discharged at 60 mA/g to the cut-off potential of −0.6 V (versus Hg/HgO). High rate dischargeability (HRD) was measured by a ratio of the discharge capacity at a given discharge current density (300–1200 mA/g) to the discharge capacity at 60 mA/g. Linear polarization curves were performed on a EG&G PARC's Model 273 Potentiostat/Galvanostat station by scanning the electrode potential at the rate of 0.1 mV/s from −5 to 5 mV (versus open circuit potential) at 50% depth of discharge (DOD), and potential step experiments were performed on the same instrument at 100% charge state. Electro-

* Corresponding author. Tel.: +86 25 83587243; fax: +86 25 83240205.
** Corresponding author. Tel.: +86 431 85262447; fax: +86 431 85262447.
E-mail addresses: maliqun@njut.edu.cn (L. Ma), lmwang@ciac.jl.cn (L. Wang).

0925-8388/$ – see front matter © 2010 Elsevier B.V. All rights reserved.
doi:10.1016/j.jallcom.2010.11.132

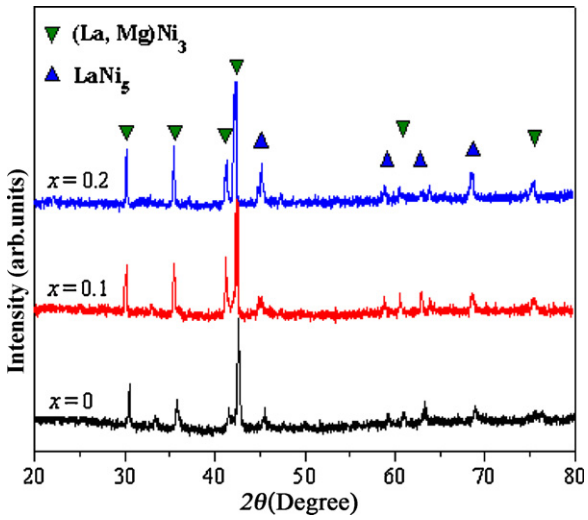

Fig. 1. XRD patterns of $La_{0.7}Mg_{0.3-x}Ca_xNi_{2.8}Co_{0.5}$ (x = 0–0.10) hydrogen storage alloys.

chemical impedance spectra (EIS) were obtained in the frequency range from 10 kHz to 1 mHz at 50% DOD.

3. Results and discussion

3.1. Microstructures

The XRD patterns of $La_{0.7}Mg_{0.3-x}Ca_xNi_{2.8}Co_{0.5}$ (x = 0–0.10) hydrogen storage alloys are shown in Fig. 1. It can be seen that the patterns exhibit similar diffraction peaks, and all alloys mainly consist of (La, Mg)Ni_3 and $LaNi_5$ phases, which indicates that the microstructures are almost unchanged by increasing x.

The lattice parameters and unit cell volumes of (La, Mg)Ni_3 and $LaNi_5$ phases in the alloys are listed in Table 1. As increasing x, the a, c and v of (La, Mg)Ni_3 phase increase, which is ascribed to that the atomic radius of Ca (1.74 Å) is larger than that of Mg (1.60 Å), whereas the a, c and v of $LaNi_5$ phase decrease, which is ascribed to that of Ca can exist in (La, Mg)Ni_3 or $LaNi_5$ phases unlike Mg [6], thus the lattice parameters of $LaNi_5$ phase decrease when Ca adds into $LaNi_5$ phase to replace La (1.88 Å). The abundances of the phases are calculated by Rietveld refinement and also listed in Table 1. It can be found the abundance of (La, Mg)Ni_3 phase decreases while the abundance of $LaNi_5$ phase increases, which is ascribed to that Ca can exist randomly in AB_5 or AB_2 structural units and Mg can only exist in AB_2 structural unit [6], thus the abundance of (La, Mg)Ni_3 phase decreases and the abundance of $LaNi_5$ phase increases.

Table 2
Summary of electrochemical characteristics for the alloy electrodes.

x	N[a]	C_{max} (mAh/g)	C_{100} (mAh/g)	S_{100} (%)	HRD_{1200} (%)
x = 0	3	387.3	179.6	46.4	60.5
x = 0.05	3	384.2	208.6	54.3	65.1
x = 0.10	3	345.4	149.3	43.2	68.5

[a] The cycle numbers needed to activate the alloy electrodes.

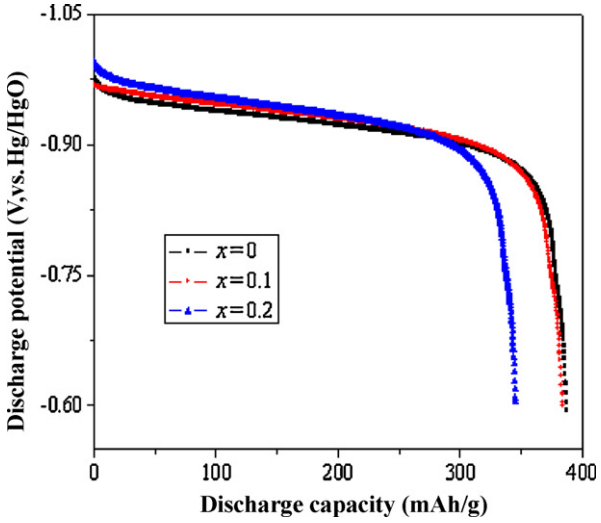

Fig. 2. Evolution of discharge potential for the alloy electrodes at 298 K.

3.2. Discharge capacity and cycle stability

The cycle numbers for activating $La_{0.7}Mg_{0.3-x}Ca_xNi_{2.8}Co_{0.5}$ (x = 0–0.10) alloy electrodes are listed in Table 2. It can be seen that the alloy electrodes can be activated to maximum discharge capacities within three cycles. Fig. 2 shows the discharge potential curves of the alloy electrodes for the third cycle. It can be obviously noted that the discharge plateau shifts towards a more positive potential with the increase of Ca, which indicates that Ca leads to an increase in discharge potential for the alloy electrodes due to its more negative electro-negativity.

The maximum discharge capacities (C_{max}) decrease from 387.3 mAh/g (x = 0) to 345.4 mAh/g (x = 0.10), which is ascribed to that the abundance of (La, Mg)Ni_3 phase decreases and the abundance of $LaNi_5$ phase increases, and it is believed that the discharge capacity of (La, Mg)Ni_3 phase is larger than that of $LaNi_5$ phase. Therefore, the maximum discharge capacities of the alloy electrodes decrease by increasing Ca content.

The relationship between discharge capacity and cycle number for the alloy electrodes is represented in Fig. 3. The cycle stability after 100 charge/discharge cycles (S_{100}) at 60 mA/g is listed in Table 2. It can be seen that the S_{100} of the alloy

Table 1
Characteristics of (La, Mg)Ni_3 and $LaNi_5$ phases in $La_{0.7}Mg_{0.3-x}Ca_xNi_{2.8}Co_{0.5}$ (x = 0–0.10) alloys.

x	Phase	Phase type	Lattice parameter (Å)		Cell volume (Å^3)	Phase abundance[a] (wt.%)
			a	c		
x = 0	(La, Mg)Ni_3	$PuNi_3$	5.055	24.635	550.1	83.17
	$LaNi_5$	$CaCu_5$	5.021	3.983	87.1	16.83
x = 0.05	(La, Mg)Ni_3	$PuNi_3$	5.059	24.711	553.7	81.52
	$LaNi_5$	$CaCu_5$	5.015	3.971	86.6	18.48
x = 0.10	(La, Mg)Ni_3	$PuNi_3$	5.077	24.843	556.2	77.81
	$LaNi_5$	$CaCu_5$	5.011	3.962	86.1	22.19

[a] Phase abundances of the phases are calculated by Rietveld refinement.

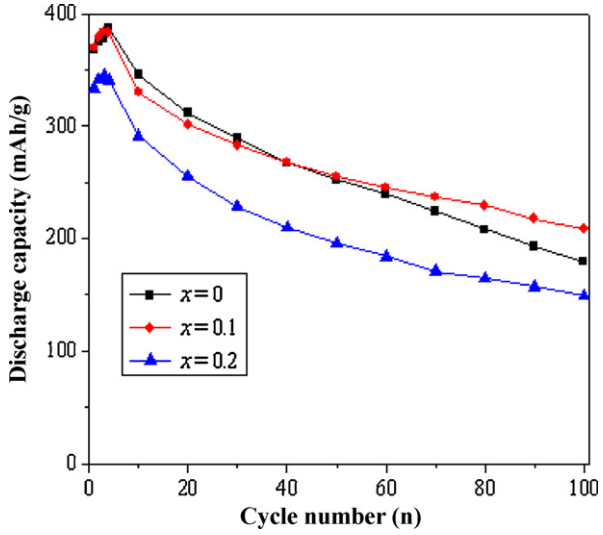

Fig. 3. Cycle stability of the alloy electrodes after 100 charge/discharge cycles.

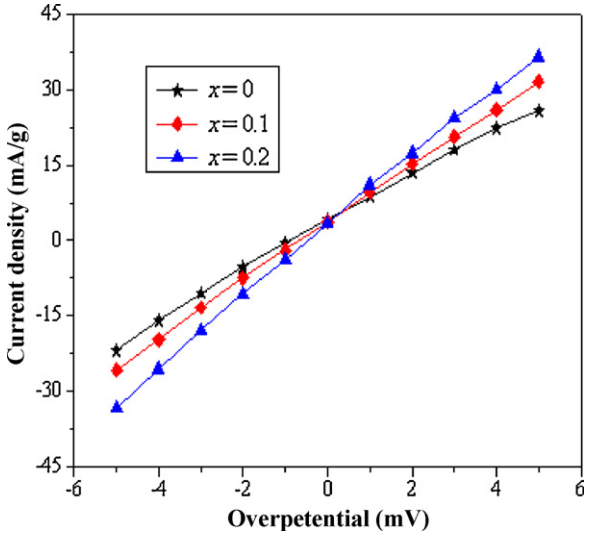

Fig. 5. Linear polarization patterns of the alloy electrodes at 50% DOD.

electrodes first increases obviously from 46.4% ($x=0$) to 54.3% ($x=0.05$), then decreases to 43.2% ($x=0.10$). The cycle behavior of $La_{0.7}Mg_{0.3-x}Ca_xNi_{2.8}Co_{0.5}$ ($x=0$–0.10) alloy electrodes can be classified into three stages: corroding stage of Ca, Mg and La, respectively. Ca is first corroded due to the most negative electronegativity, which prevents Mg and La from corrosion and results in the improvement of cycle stability. However, excessive Ca content ($x=0.10$) accelerates the corrosion rate of the alloy electrodes and leads to declining the cycle stability. Accordingly, the cycle stability of the alloy electrodes first increases and then decreases with the increase of Ca.

3.3. High rate dischargeability and electrochemical kinetics

Fig. 4 represents the relationship between the high rate dischargeability (HRD) and discharge current density of $La_{0.7}Mg_{0.3-x}Ca_xNi_{2.8}Co_{0.5}$ ($x=0$–0.10) alloy electrodes. HRDs at the discharge current density of 1200 mA/g are listed in Table 2. It can be seen that the HRD_{1200} increases from 64.5% ($x=0$) to 68.5% ($x=0.10$), which is ascribed to that the mass fraction of electrocatalytic Ni on the alloy surface increases with the dissolution of Ca in KOH solution and the electro-catalytic Ni can promote the diffusion of hydrogen.

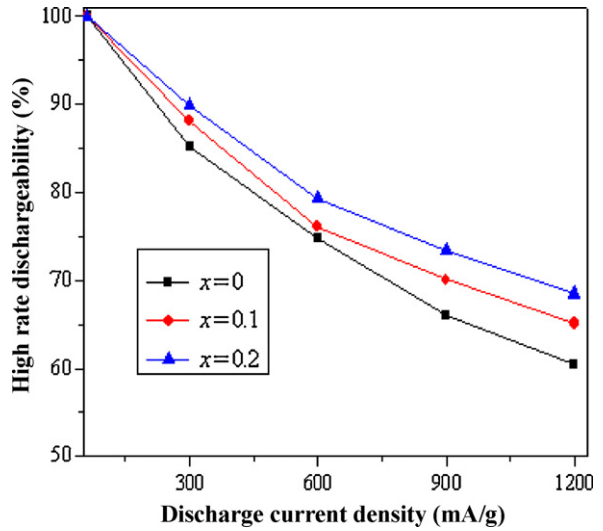

Fig. 4. High rate dischargeability of the alloy electrodes at 298 K.

It is generally accepted that HRDs of metal hydride electrode are determined by polarization current density I_0 and diffusion coefficient of hydrogen D [7,8]. Fig. 5 exhibits linear polarization curves of the alloy electrodes at 50% DOD. There is a linear dependence between current density and overpotential within a small overpotential range (±5 mV). Based on the measured curves, values of polarization current density I_0 and polarization resistance R_p are calculated by the following formula [9–12]:

$$I_0 = \frac{RT}{FR_p} \tag{1}$$

where R is the gas constant, T is the absolute temperature, F is the Faraday constant, and R_p is the polarization resistance. The I_0 values obtained from Eq. (1) are tabulated in Table 3. It is found that the I_0 increase from 219.7 mA/g ($x=0$) to 258.8 mA/g ($x=0.10$).

The potential step curves of the alloy electrodes are shown in Fig. 6. The hydrogen diffusion coefficient D can be calculated by the following equation [13–15]:

$$\log(i) = \log\left(\frac{6FD(c_0 - c_s)}{da^2}\right) - \left(\frac{\pi^2 t}{2.303}\right)\left(\frac{D}{a^2}\right) \tag{2}$$

where D is the hydrogen diffusion coefficient (cm^2/s), a is the radius of the spherical particle (cm), i is the diffusion current density (A/g), c_0 is the initial hydrogen concentration in the bulk electrode (mol/cm^3), c_s is the hydrogen concentration on the surface of alloy particles (mol/cm^3), d is the density of the hydrogen storage materials (g/cm^3), and t is the discharge time. The hydrogen diffusion coefficient D in the bulk electrodes is estimated by Eq. (2) and listed in Table 3. It is shown that the D increases from 9.6×10^{-11} cm^2/s ($x=0$) to 10.1×10^{-11} cm^2/s ($x=0.10$).

Iwakura et al. [16] have reported that a linear dependence of high rate dischargeability on polarization current density is observed when electrochemical reaction on alloy surface is the rate-determining factor. Otherwise, high rate dischargeability is

Table 3
Summary of kinetic parameters of the alloy electrodes at 298 K.

x	I_0 (mA/g)	R_p (mΩ)	D (cm^2/s)	R_{ct} (mΩ)
$x=0$	219.7	116.9	9.6×10^{-11}	138.6
$x=0.05$	242.6	105.8	9.8×10^{-11}	110.2
$x=0.10$	258.8	99.2	10.1×10^{-11}	95.7

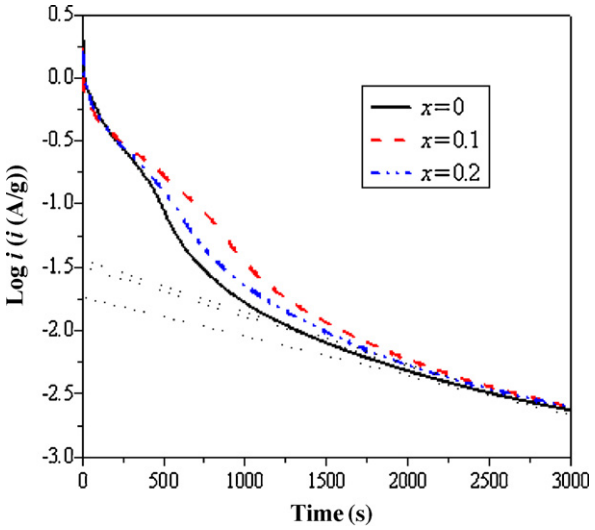

Fig. 6. Potential step curves of the alloy electrodes at 298 K.

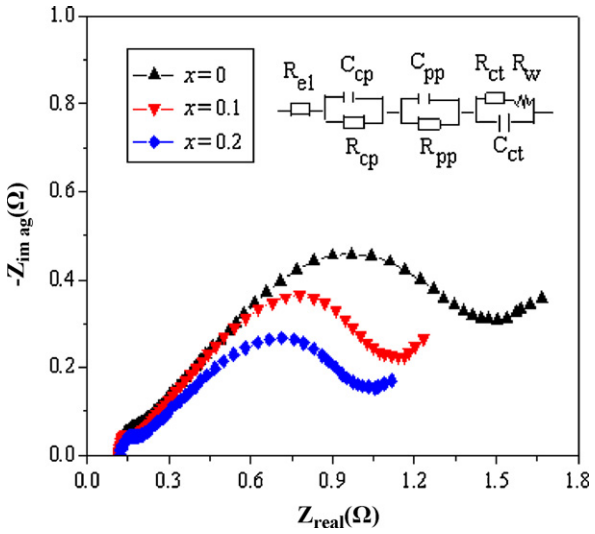

Fig. 8. Electrochemical impedance spectra of the alloy electrodes at 50% DOD.

constant when diffusion rate of hydrogen in alloy bulk is the rate-determining factor. Fig. 7 represents that the HRD_{1200} is a linear function with I_0. Accordingly, the HRD_{1200} is essentially controlled by charge-transfer reaction of hydrogen on alloy surface at the discharge current density of 1200 mA/g.

3.4. Electrochemical impedance spectroscopy

The EIS of $La_{0.7}Mg_{0.3-x}Ca_xNi_{2.8}Co_{0.5}$ (x = 0–0.10) alloy electrodes at 50% depth of discharge (DOD) is shown in Fig. 8. Each spectroscopy consists of a small semicircle in high frequency region and a large semicircle in low frequency region and a straight line. According to the model proposed by Kuriyama et al. [17], the small semicircle in EIS curve indicates the contact resistance between alloy powder and conductive material, and the large semicircle represents the charge-transfer resistance (R_{ct}) on alloy electrode surface. The large semicircle in low frequency region decreases during charge/discharge cycles in Fig. 8, which is due to the dissolution of Ca in KOH solution and a consequent increase of mass fraction for the electro-catalytic Ni on the alloy surface.

The EIS data is analyzed using an equivalent circuit represented by the inset. The R_{ct} values of the alloy electrodes, summarized in Table 3, decrease from 138.6 mΩ (x = 0) to 95.7 mΩ (x = 0.10), which indicates that the charge-transfer reaction on alloy electrode surface becomes faster with the increase of Ca. The results illustrate that the HRDs are essentially controlled by charge-transfer reaction of hydrogen on alloy surface once again, which is ascribed to that the mass fraction of electro-catalytic Ni on the alloy surface increases with the dissolution of Ca in KOH solution and the electro-catalytic Ni can promote the diffusion of hydrogen.

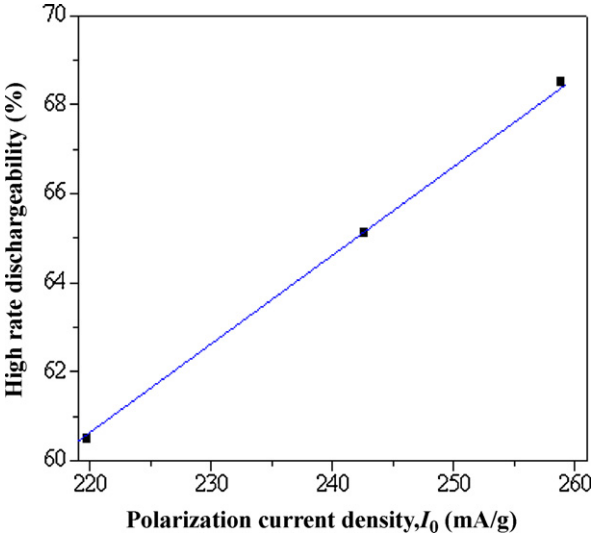

Fig. 7. HRD_{1200} as a function of I_0 of the alloy electrodes at 298 K.

4. Conclusion

The microstructure and electrochemical properties of $La_{0.7}Mg_{0.3-x}Ca_xNi_{2.8}Co_{0.5}$ (x = 0–0.10) hydrogen storage alloys are investigated in this work. All alloys consist of (La, Mg)Ni_3 and $LaNi_5$ phases. As increasing Ca content, the maximum discharge capacity of the alloy electrodes decreases, the HRD_{1200} increases and the cycle stability (S_{100}) first increases and then decreases. The electrochemical impedance spectroscopy results indicate that the electrochemical kinetics of the alloy electrodes is also improved by increasing x. All results exhibit that the electro-negativity and reactive activity of Ca are two important factors to influence the overall electrochemical hydrogen storage properties of $La_{0.7}Mg_{0.3-x}Ca_xNi_{2.8}Co_{0.5}$ (x = 0–0.10) alloys.

Acknowledgements

This work was financially supported by the National High Technology Research and Development Program of China (2007AA03Z228), the Project supported by the Major program for the fundamental research of the Chinese Academy of Sciences (KJCX2-Y1W-H21), the Science and Technology Cooperation Project of Chinese Academy of Sciences and Jilin Province (2008syhz0008), the NSFC fund for Creative Research Group (20921002) and the Open Subject of State Key Laboratory of Rare Earth Resource Utilization.

References

[1] K. Kadir, T. Sakai, I. Uehare, J. Alloys Compd. 302 (2000) 112.
[2] J. Chen, N. Kuriyama, H.T. Takeshita, H. Tanaka, T. Sakai, M. Haruta, Electrochem. Solid-State Lett. 3 (2000) 249.
[3] Y.X. Liu, L.Q. Xu, W.Q. Jiang, G.X. Li, W.L. Wei, J. Guo, Int. J. Hydrogen Energy 34 (2009) 2986.
[4] Y. Li, S.M. Han, J.H. Li, X.L. Zhu, L. Hu, Mater. Chem. Phys. 108 (2008) 92.
[5] Z.W. Dong, Y.M. Wu, L.Q. Ma, X.D. Shen, L.M. Wang, Mater. Res. Bull. 45 (2010) 256.

[6] P. Zhang, Y.N. Liu, R. Tang, J.W. Zhu, X.D. Wei, S.S. Liu, G. Yu, Electrochim. Acta 51 (2006) 6400.
[7] T. Sakai, H. Miyamura, N. Kuriyama, A. Kato, K. Oguro, H. Ishikawa, C. Iwakura, J. Less-Common Met. 159 (1990) 127.
[8] X.B. Zhang, D.Z. Sun, W.Y. Yin, Y.J. Chai, M.S. Zhao, Electrochim. Acta 50 (2005) 3407.
[9] P.H.L. Notten, P. Hokkeling, J. Electrochem. Soc. 138 (1991) 1877.
[10] X.Q. Shen, Y.G. Chen, M.D. Tao, C.L. Wu, G. Deng, Z.Z. Kang, Int. J. Hydrogen Energy 34 (2009) 2661.
[11] H.G. Pan, S. Ma, J. Shen, J.J. Tan, J.L. Deng, M.X. Gao, Int. J. Hydrogen Energy 32 (2007) 2949.
[12] F.L. Zhang, Y.C. Luo, D.H. Wang, R.X. Yan, L. Kang, J.H. Chen, J. Alloys Compd. 439 (2007) 181.
[13] Y. Li, D. Han, S.M. Han, X.L. Zhu, L. Hu, Z. Zhang, Y.W. Liu, Int. J. Hydrogen Energy 34 (2009) 1399.
[14] W. Hu, J.L. Wang, L.D. Wang, Y.M. Wu, L.M. Wang, Electrochim. Acta 54 (2009) 2770.
[15] G. Zheng, B.N. Popov, R.E. White, J. Electrochem. Soc. 142 (1995) 154.
[16] C. Iwakura, T. Oura, H. Inoue, M. Matsuoka, Electrochim. Acta 41 (1996) 117.
[17] N. Kuriyama, T. Sakai, H. Miyamura, I. Uehara, H. Ishikawa, T. Iwasaki, J. Electrochem. Soc. 139 (1992) L72.